Journal of Catalysis 301 (2013) 77–82

Contents lists available at SciVerse ScienceDirect

Journal of Catalysis

journal homepage: www.elsevier.com/locate/jcat

Identification of $Fe_2(\mu\text{-}O)$ and $Fe_2(\mu\text{-}O)_2$ sites in Fe/ZSM-35 by *in situ* resonance Raman spectroscopy

Junying Wang [a,b], Guanna Li [a], Xiaohua Ju [a], Haian Xia [a], Fengtao Fan [a], Junhu Wang [a], Zhaochi Feng [a,*], Can Li [a,*]

[a] State Key Laboratory of Catalysis, Dalian Institute of Chemical Physics, Chinese Academy of Sciences, 457 Zhongshan Road, Dalian 116023, China
[b] Graduate University of Chinese Academy of Sciences, Beijing 100049, China

ARTICLE INFO

Article history:
Received 28 September 2012
Revised 29 December 2012
Accepted 25 January 2013

Keywords:
Resonance Raman spectroscopy
Fe/ZSM-35
Active iron site

ABSTRACT

The structure of the active iron site in Fe/ZSM-35 was investigated by *in situ* resonance Raman spectroscopy combined with Mössbauer spectroscopy and DFT calculations. *In situ* UV resonance Raman spectra coupled with ^{57}Fe Mössbauer spectra suggest that the active Fe site for N_2O decomposition is an $Fe_2(\mu\text{-}O)$ site, characterized by a Raman band at 875 cm^{-1}. *In situ* visible resonance Raman spectra reveals the formation of an $Fe_2(\mu\text{-}O)_2$ site with a feature Raman band at 730 cm^{-1} upon N_2O reacts with the $Fe_2(\mu\text{-}O)$ site. The Raman band intensity at 730 cm^{-1} is decreasing after exposing the $Fe_2(\mu\text{-}O)_2$ site to CH_4 due to the formation of methoxide species which mimics the biocatalysis of soluble methane monooxygenase (sMMO).

1. Introduction

Fe/ZSM-35 has been shown a promising catalyst for de-NO_x [1], and N_2O decomposition [2], and one-step benzene hydroxylation to phenol [3]. Although its catalytic properties have been extensively studied, much less research has been dedicated to elucidate the structure of the active sites. Both mono-nuclear and bi-nuclear iron sites have been proposed to be the active sites for N_2O decomposition [4,5]. Furthermore, extensive studies reveal that the iron species giving UV–visible absorption features between 300 and 400 nm is important for N_2O decomposition [6,7]. Given the heterogeneous nature and low concentration of the active sites in the zeolite, to identify the active iron site involved in N_2O decomposition is not a trivial undertaking.

Herein, we present *in situ* resonance Raman spectroscopic data that provide molecular-level insights into the structure of the active iron site. The resonance Raman effect selectively enhances the intensities of Raman bands associated with the Fe-oxo species when tuning the excitation laser into its characteristic absorption band [8,9]. *In situ* UV resonance Raman and Mössbauer spectra defined the active iron site as an $Fe_2(\mu\text{-}O)$ site, which is characterized by a Raman band at 875 cm^{-1}. Reaction of the $Fe_2(\mu\text{-}O)$ site with N_2O yields an $Fe_2(\mu\text{-}O)_2$ site, which exhibits a resonance-enhanced Raman band at 730 cm^{-1}.

2. Experimental

2.1. Catalyst preparation

Fe/ZSM-35 samples were prepared by a two-stage synthesis method. A ZSM-35 precursor suspension was synthesized using cyclohexylamine (CHA) as the structure-directing agent and Ludox HS30 as the Si source with a molar composition of 3 M_2O (M = K + Na):21 SiO_2:1 Al_2O_3:10 CHA:1600 H_2O. Ludox HS30 (12 g) was hydrolysis in a hot base solution containing 1 M NaOH (2 ml), 1 M KOH (2.6 ml), and deionized water (33 ml) under stirring to form solution A; sodium aluminate (0.68 g) was dissolved in a base solution containing 1 M NaOH solution (2 ml) and 1 M KOH solution (2.6 ml) under stirring at room temperature to form solution B. Subsequently, solution B was added dropwise into solution A under very vigorous stirring at room temperature, and then, CHA (3.3 ml) was added to the mixture. After thorough homogenization, the smooth gel was transferred to a Teflon-coated stainless-steel autoclave and was subjected to hydrothermal treatment under static conditions at 493 K for 20 h. A Fe/ZSM-35 precursor suspension was prepared following the same procedure but with a molar composition of 3 M_2O (M = K + Na):21 SiO_2:1 (Al_2O_3 + Fe_2O_3):10 CHA:1600 H_2O, in which SiO_2/Fe_2O_3 molar ratios varied from 40 to 160. A required quantity of the ferric chloride solution (1 M) was added after mixing the aluminate and silica solutions,

* Corresponding authors. Fax: +86 411 84694447.
E-mail addresses: zcfeng@dicp.ac.cn (Z. Feng), canli@dicp.ac.cn (C. Li).
URL: http://www.canli.dicp.ac.cn (C. Li).

0021-9517/$ - see front matter Crown Copyright © 2013 Published by Elsevier Inc. All rights reserved.
http://dx.doi.org/10.1016/j.jcat.2013.01.023

and crystallization was carried out at 493 K for 5 h. After the pre-crystallization step, the collected liquid phases were mixed together and the collected solid phases were grinded together for a few minutes. Finally, the resultant mixture was transferred into a Teflon-lined stainless-steel autoclave and kept under static conditions and autogenous pressures at 493 K for 14 h. The resulting solid was recovered by filtration, washed in deionized water, and dried at 353 K overnight. Calcination was performed at 823 K in air for 10 h. The calcined materials were converted into the H-form by ion-exchange with a 1 M NH_4NO_3 solution three times and followed by treating at 1173 K in flowing helium for 2 h.

2.2. Catalyst characterization

The chemical composition of the Fe/ZSM-35 samples was determined by Inductive Coupled Plasma Emission Spectrometer (ICP). The experiment was done on a shimazu ICPS-8100 instrument (Table 1).

Fe/ZSM-35 samples were characterized by X-ray diffraction using the packed powder method, on a Rigaku Miniflex X-ray diffractometer with a Cu Kα monochromatic radiation at room temperature (λ = 1.5418 Å). No bulky iron oxides were detected (see Fig. 1).

UV–visible diffuse reflectance spectra (UV–visible DRS) were recorded on a JASCO V-550 spectrometer equipped with an integrating sphere coated by $BaSO_4$. $BaSO_4$ was used as a reference material.

In situ UV resonance Raman spectra were obtained on a home-made UV Raman spectrograph with a triple-stage spectrograph at a resolution of 2 cm^{-1}. The laser line at 325 nm emitted from a KIMMON IK-3351 R-G He–Cd laser was used as an exciting source. The power of the laser at samples was about 1.0 mW. The samples were pressed into self-supporting wafers (~15 mg cm^{-2}) and introduced into an *in situ* quartz cell. The high-temperature-treated sample wafers were firstly calcined at 823 K in a flow of O_2 for 1 h followed by treating at 1173 K in flowing He for 1 h. The *in situ* Raman cell was closed and cooled to room temperature, and then, the spectra were recorded.

In situ visible resonance Raman spectra were collected on a home-assembled UV–visible Raman spectrograph. The excitation laser lines at 457, 532, and 671 nm from three different semiconductor lasers were used as excitation source. The scattered photons were collected in a back-scattering geometry. Details of the experimental processes were described as follows: first, the sample was pressed into self-supporting wafers and placed in an *in situ* quartz cell equipped with gas inlet/outlet ports and heater. Second, the samples were pretreated at 823 K in flowing O_2 for 1 h followed by activating at 1173 K in flowing He for 1 h. Finally, the samples were cooled to 523 K and then a flowing N_2O/He (5.0 vol%) mixed gas was introduced into the cell. After each treatment, the cell was quickly sealed and cooled to room temperature and the Raman

Table 1
The concentration of active iron sites determined by N_2O decomposition at 523 K for the high-temperature-activated Fe/ZSM-35 samples.

Sample	Fe (wt.%)	Fe(II) sites ($\times 10^{19}$ sites, g^{-1})	Fe(II)/Fe_{total}	SSA[a] (m^2 g^1)	Fe(II) sites[b] ($\times 10^{17}$ sites, m^{-2})
Fe/ZSM-35 (Si/Fe = 80)	0.76	7.76	0.95	333	2.33
Fe/ZSM-35 (Si/Fe = 160)	0.45	4.57	0.94	361	1.27
Fe/ZSM-35 (Si/Fe = 320)	0.32	3.24	0.94	348	0.93

[a] Measured by multipoint BET method at −196 °C, expressed per g of sample.
[b] Concentration of active iron sites normalized by the surface area of Fe/ZSM-35 samples with different Si/Fe ratios.

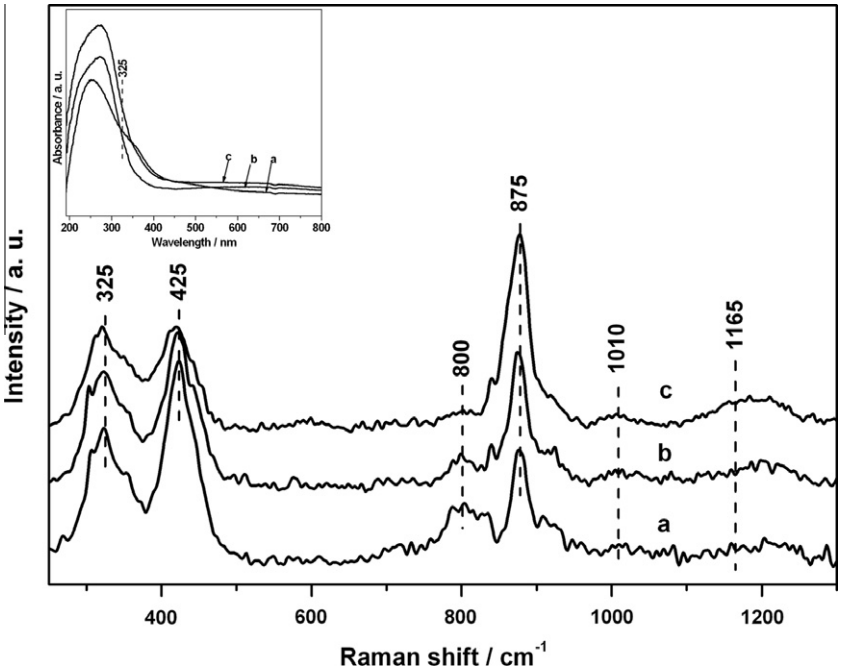

Fig. 1. *In situ* UV resonance Raman spectra of the high-temperature-treated Fe/ZSM-35 samples. The excitation laser line: 325 nm. Inset: UV–visible DRS of the high-temperature-treated Fe/ZSM-35 samples. (a) Si/Fe = 320, (b) Si/Fe = 160, and (c) Si/Fe = 80.

spectrum was recorded. The acquisition time was 10 min with spectral resolution of 2 cm^{-1}. The power of the 532 nm excitation laser line at samples was about 3.0 mW. The samples were not damaged in view of the invariance of the spectra during data acquisition.

^{57}Fe Mössbauer spectra were measured at 298 K on a spectrometer working in the mode of constant accelerations with the use of ^{57}Co: Rh source. Data analysis involved a least-square fitting procedure made by assuming a Lorentzian peak shape and employing the fitting program MössWin. The isomer shifts (IS) values were given relatively to iron foil at room temperature.

The method applied to determine the concentration of active iron sites is similar to the transient response technique adopted by Kiwi-Minsker et al. [10]. Firstly, the catalysts were treated in helium flow at 1173 K for 1 h followed by cooling to 523 K in a flow of helium. Then, the reactor effluent was continuously monitored after a step change from a flow of pure helium to N_2O/He (5.0 vol%) at 523 K on the high-temperature-treated Fe/ZSM-35 samples. The amount of active iron sites was quantified by integration of N_2 peak area on the basis of the assumption that one active iron site is occupied by one oxygen atom.

2.3. Activity measurements

For catalytic nitrous oxide decomposition, a standard U-shaped flow reactor with an inner diameter of 4 mm was used. About 50 mg catalyst was held between two quartz wool plugs. The feed gas was 5.0 vol% N_2O in helium at a GHSV of 24,000 h^{-1}. An on-line mass spectrometer (Gam 200, Pfeiffer Vacuum) calibrated by gases of known composition was used for quantitative analysis of gas-phase concentrations.

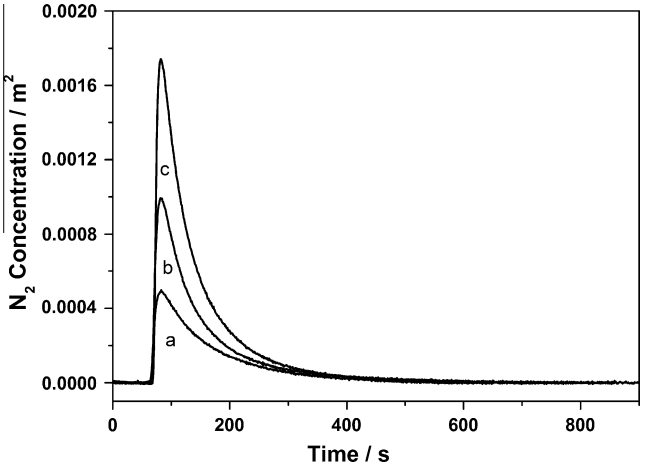

Fig. 2. Relationship between the N_2 concentration normalized by the surface area with different Si/Fe ratios of high-temperature-treated Fe/ZSM-35 samples and the reaction time after a step change from helium to N_2O/He (5.0 vol%). (a) Si/Fe = 320, (b) Si/Fe = 160, and (c) Si/Fe = 80.

2.4. Periodic DFT calculations

All the DFT calculations were performed using Gaussian 03 D.01 code [11] with the B3LYP [12,13] hybrid exchange–correlation functional and 6-31++g(d, p) basis set. Harmonic vibrational analysis was performed based on the optimized geometries. Bi-nuclear $[Fe(\mu\text{-}O)Fe]^{II}$, $[Fe(\mu\text{-}O)_2Fe]^{II}$ active sites were proposed for the calculation. The starting geometry of the clusters corresponded to the real lattice of the FER zeolite corresponding to X-ray diffraction data [14]. Substitution of Al atoms over FER zeolite, as well as stability of iron-containing active site, was studied using $Fe_2Al_2Si_2O_{15}$-H_{10} cluster models, which represent the wall of the 10-membered ring of straight channel. $[Fe(\mu\text{-}O)Fe]^{II}$ and $[Fe(\mu\text{-}O)_2Fe]^{II}$ cations compensated the negative charge of the two $[AlO_2]^{I}$ unit. Al atoms were placed in T4 lattice positions. Hydrogen atoms oriented to the next Si sites were used to saturate the dangling Si–O bonds at the periphery of the cluster. All of the atoms of the cluster were allowed to relax with the exception of the terminal H atoms.

3. Results and discussion

3.1. In situ UV resonance Raman spectra of the high-temperature-treated Fe/ZSM-35 samples

In situ UV resonance Raman spectra were collected for the high-temperature-treated Fe/ZSM-35 samples with 325-nm excitation. Besides the characteristic Raman bands at 325, 425, and 800 cm^{-1} for the ZSM-35 zeolite lattice [15–17], three new Raman bands at 875, 1010, and 1165 cm^{-1} are observed (Fig. 1). The Raman bands at 1010 and 1165 cm^{-1} are assignable to the asymmetric stretching vibrations of isolated Fe–O–Si entities at extraframework or in framework positions [18–20]. The Raman band at 875 cm^{-1} is ascribed to the ν_{as} (Fe–O–Fe), which falls in the range of 725–885 cm^{-1} reported for Fe–O–Fe asymmetric stretching vibrations of μ-oxodiiron complexes [21–23]. The Raman spectra show that the intensity of the Raman band at 875 cm^{-1} increases with increasing Fe/Si molar ratios (Fig. 1, trace a, b, and c). This trend is consistent with the transient response results which show that the number of active Fe sites increases with increasing Fe/Si atomic ratios (Fig. 2 and Table 1). It is noted that the rate of N_2O decomposition also increases with increasing intensity ratio of the band at 875 cm^{-1} to that at 425 cm^{-1}

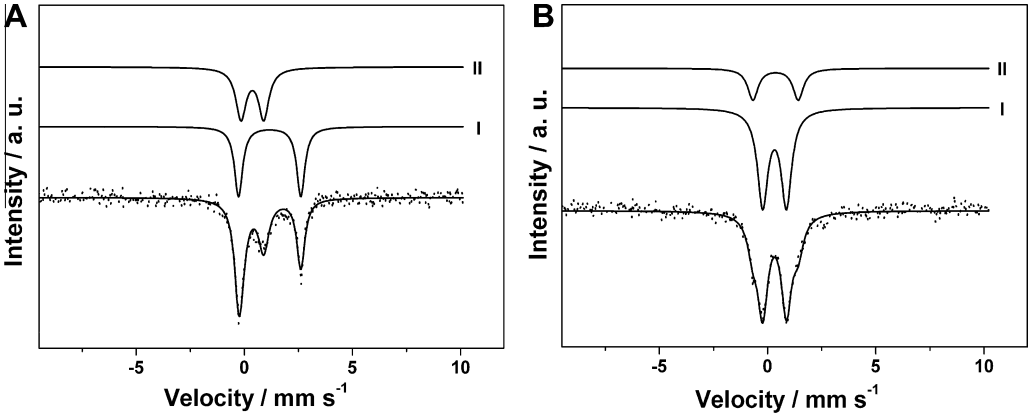

Fig. 3. Room temperature ^{57}Fe Mössbauer spectra of (A) high-temperature-treated Fe/ZSM-35 (Si/Fe = 80) sample and (B) after exposing (A) to N_2O/He (5.0 vol%) at 523 K.

Table 2
^{57}Fe Mössbauer parameters of the Fe/ZSM-35 (Si/Fe = 80) sample at room temperature.

Catalyst	Fe state	Spectral parameters (mm s^{-1})			
		Isomer shift[a]	Quadrupole splitting[b]	Spectral Contribution (%)[c]	FWHM[d] (mm s^{-1})
Fe/ZSM-35	Fe(II)–Fe(II)	1.17	2.88	52	0.45
(1173 PC/He)	Fe(III)–Fe(III)	0.37	1.05	48	0.58
Fe/ZSM-35	Fe(Iir)–Fe(III)	0.32	1.10	75	0.58
(1173 K/He + O_a)	Fe(III)–Fe(III)	0.37	2.09	25	0.58

[a] Isomer shift, relative to α-Fe at room temperature.
[b] Quadrupole splitting, electric quadrupole splitting.
[c] Relative resonance areas of the different components of the absorption patterns.
[d] Full-line width at half maximum: uncertainty is ±5% of the reported values.

(Fig. S1), suggesting that the Fe site characterized by the Raman band at 875 cm^{-1} is the active site for N_2O decomposition.

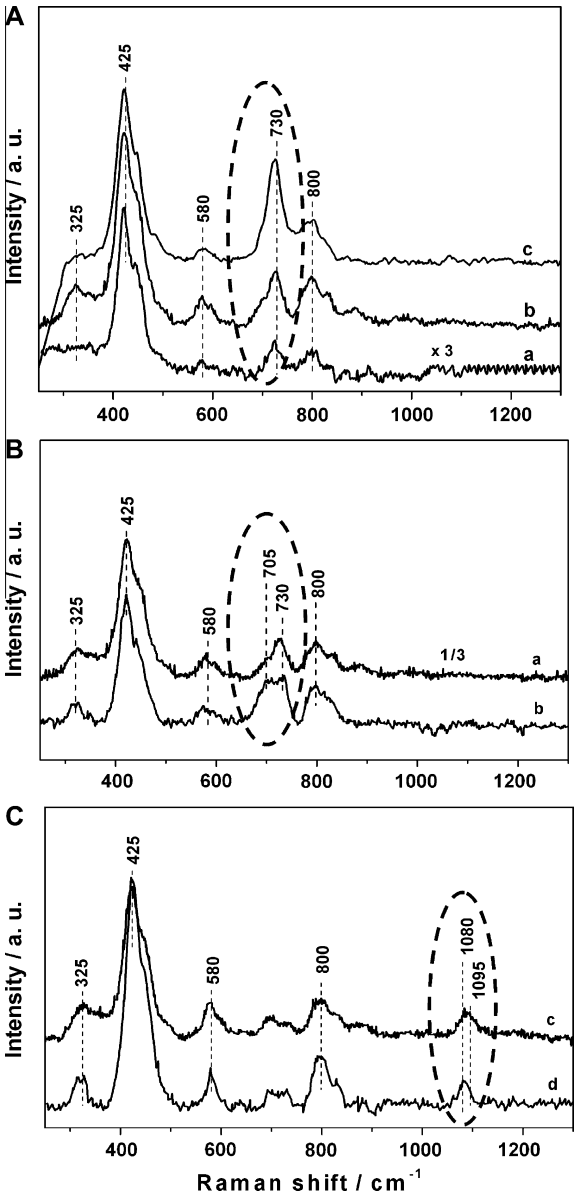

Fig. 4. *In situ* visible resonance Raman spectra of N_2O-activated Fe/ZSM-35 (Si/Fe = 80) sample. (A) *In situ* visible resonance Raman spectra of $^{14}N_2{}^{16}O$/He (5.0 vol%)-activated Fe/ZSM-35 collected at three excitation laser lines: (a) λ_{ex} = 671 nm, (b) λ_{ex} = 532 nm, and (c) λ_{ex} = 457 nm. (B) *In situ* visible resonance Raman spectra (λ_{ex} = 532 nm) of (a) $^{14}N_2{}^{16}O$/He (5.0 vol%)-activated Fe/ZSM-35 sample, (b) $^{15}N_2{}^{18}O$/He (1.0 vol%)-activated Fe/ZSM-35 sample. (C) *In situ* visible resonance Raman spectra (λ_{ex} = 532 nm) of (c) exposing (a) to methane (10.0 vol%) at room temperature, (d) exposing (b) to methane (10.0 vol%) at room temperature.

3.2. ^{57}Fe Mössbauer spectra of the high-temperature-treated Fe/ZSM-35 sample

A Mössbauer study was performed to gain further information concerning the detailed nuclearity and oxidation states of the active iron site. The Mössbauer spectrum of Fe/ZSM-35 (Si/Fe = 80) is fitted by two doublet subspectra with IS = 1.17 mm s^{-1}, QS = 2.88 mm s^{-1} and IS = 0.37 mm s^{-1}, QS = 1.05 mm s^{-1} (Fig. 3A and (Table 2). Based on the literature data [24,25], $Fe^{(III)}$ ions located in T-sites in tetrahedral coordination are characterized by IS < 0.3 mm s^{-1} and may exhibit different QS values depending on the symmetry of coordination of ligands while those with IS > 0.3 mm s^{-1} and 0.8 < QS < 1.2 mm s^{-1} are probably due to extraframework $Fe^{(III)}$ in octahedral coordination [26]. For $Fe^{(II)}$ ions with coordination numbers 4 usually have 0.8 < IS < 1.0 mm s^{-1} and QS < 1 mm s^{-1}, whereas $Fe^{(II)}$ ions with coordination numbers 5 or 6 exhibit 1.1 < IS < 1.3 mm s^{-1} and QS > 1.5 mm s^{-1}. When the sample cooling from room temperature to 77 K, IS values increase by 0.1–0.15 mm s^{-1} [27]. Therefore, the component with IS = 0.37 mm s^{-1}, QS = 1.05 mm s^{-1} is assigned to extraframework $Fe^{(III)}$ ions in octahedral coordination. Furthermore, QS values ranging from 0.76 to 2.4 mm s^{-1} are characteristic of binuclear $Fe^{(III)}$ complexes [28]. Therefore, the spectral component with IS = 0.37 mm s^{-1}, QS = 1.05 mm s^{-1} could be assigned to binuclear $Fe^{(III)}$–O–$Fe^{(III)}$ species with octahedral coordination [28]. The presence of Fe^{III} ions is possibly due to the slow oxidation of the Fe^{II} ions on contact with atmosphere [29]. The component with IS = 1.17 mm s^{-1}, QS = 2.88 mm s^{-1} is ascribed to binuclear $Fe^{(II)}$–O–$Fe^{(II)}$ ions with coordination numbers 5 or 6 [28]. After exposing the high-temperature-treated Fe/ZSM-35 samples to N_2O at 523 K, drastic changes occurred in the Mössbauer spectrum (Fig. 3B). The spectrum was successfully deconvoluted into two new components that are typical for $Fe^{(III)}$ species with IS = 0.32 mm s^{-1}, QS = 1.10 mm s^{-1} and IS = 0.37 mm s^{-1}, QS = 2.09 mm s^{-1}, respectively (Table 2). The component with IS = 0.32 mm s^{-1}, QS = 1.10 mm s^{-1} is ascribed to binuclear $Fe^{(III)}$–O–$Fe^{(III)}$ species [28]. The large QS values (QS = 2.09 mm s^{-1}) indicate that $Fe^{(III)}$ ions are present as binuclear $Fe^{(III)}$–O–$Fe^{(III)}$ ions [28]. Thus, the component with IS = 0.37 mm s^{-1}, QS = 2.09 mm s^{-1} is due to binuclear $Fe^{(III)}$–O–$Fe^{(III)}$ species [28]. This indicates that $Fe^{(III)}$ and $Fe^{(II)}$ components were distinctly identified and paramagnetic relaxation component [30] was not obviously observed in the Fe/ZSM-35 samples investigated. This is probably due to the differences in sample preparation methods and pretreatment conditions. Hence, from *in situ* UV resonance Raman and Mössbauer studies, we conclude that the active iron site giving a feature Raman band at 875 cm^{-1} is an $Fe_2(\mu$-O) site.

3.3. In situ visible resonance Raman spectra of N_2O-activated Fe/ZSM-35 sample

In order to get clear features of the oxygen species generated upon reaction of Fe/ZSM-35 with N_2O, resonance Raman measure-

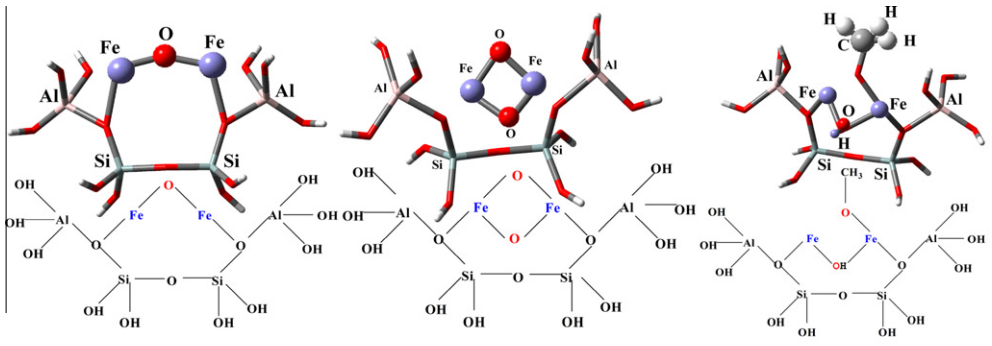

D

Experimental ($\Delta\ ^{18}O_2$) / cm^{-1}	DFT ($\Delta\ ^{18}O_2$) / cm^{-1}	Assignment
875 (-)	878 (-)	ν_{as} (Fe–O-Fe)
730 (-25)	746 (-24)	ν_s ($Fe_2(\mu\text{–}O)_2$)
1095 (-15)	1067 (-29)	ν_s (C–O)

Fig. 5. Periodic DFT-optimized structure of (A) the $Fe_2(\mu$-O) site, (B) the $Fe_2(\mu$-$O)_2$ site, and (C) Fe-methoxide species. (D) Comparison of experimentally observed Raman bands with DFT calculated vibrational frequencies (^{18}O-isotopic shifts in parentheses) of (A), (B), and (C).

ments were performed for the oxygen species generated with both N_2O and $^{15}N_2{}^{18}O$, except for the Raman bands at 325, 425, and 800 cm^{-1}, which are characteristics of the ZSM-35 framework vibrations. Two new Raman bands at 580 and 730 cm^{-1} were obtained. The Raman band at 580 cm^{-1} probably stems from (Fe–O) bending vibration of bi- or oligonuclear iron clusters [31]. The resonance Raman spectra obtained by varying the excitation laser line from 671 nm to 457 nm (Fig. 4A) suggesting that excitation in or near resonance with the electronic transition of the oxygen species permits the observation of the Raman band at 730 cm^{-1}. The Raman band at 730 cm^{-1} disappears and a new band at 1095 cm^{-1} appears simultaneously after the oxygen species reacts with CH_4 (10.0 vol%) at room temperature (Fig. 4C-c). When the oxygen species is generated with $^{15}N_2{}^{18}O$/He (1.0 vol%), a new Raman band at 705 cm^{-1} appears, and the intensity of the Raman band at 730 cm^{-1} decreases dramatically (Fig. 4B-b). Both the Raman bands at 705 and 730 cm^{-1} can be observed after exposure of the high-temperature-treated Fe/ZSM-35 sample to $^{15}N_2{}^{18}O$/He (1.0 vol%) at 523 K is probably due to the fact that about 50–75% of ^{18}O oxygen captured during decomposition of N_2O at 200–400 °C over Fe-FER can be exchanged by abundantly present zeolite lattice ^{16}O oxygen [32,33]. The intensity of the Raman band at 730 cm^{-1} generated by $^{15}N_2{}^{18}O$/He (1.0 vol%) decreases compared to the Raman band at 730 cm^{-1} generated by N_2O/He (5.0 vol%) is probably originated from the fact that the concentration of the $^{15}N_2{}^{18}O$/He (1.0 vol%) gas is much lower than that of the N_2O/He (5.0 vol%) gas.

Reaction of the $^{15}N_2{}^{18}O$-generated oxygen species with CH_4 downshifts the Raman band at 1095 cm^{-1} to that at 1080 cm^{-1} ($\Delta(^{18}O) = -15$ cm^{-1}) (Fig. 4C-d). The band at 1095 cm^{-1} is due to symmetric (C–O) stretching vibrations of methoxide species bound to Fe sites [34]. The observed resonance Raman bands and ^{18}O shifts (−25 cm^{-1}) are in agreement with the symmetric stretching vibrations of $Fe_2(\mu$-$O)_2$ in synthetic Fe-containing complexes (725–850 cm^{-1}) [21,22] and allow us to ascribe the 730 cm^{-1} band to an $Fe_2(\mu$-$O)_2$ site. Although the ν_{as} (Fe–O–Fe) vibrations (band at 875 cm^{-1}) are not detected in the *in situ* visible resonance Raman spectra of the active oxygen species, it is reasonable to assume that the μ-oxo bridge, present in the high-temperature-treated Fe/ZSM-35 samples, still remains. From *in situ* UV and visible resonance Raman and Mössbauer studies, we conclude that the active oxygen species with a feature Raman band at 730 cm^{-1} is probably an $Fe_2(\mu$-$O)_2$ site.

3.4. Periodic DFT calculations

To further clarify these experimental observations, we performed DFT calculations on the active $Fe_2(\mu$-O) site, the active $Fe_2(\mu$-$O)_2$ site, and Fe-methoxide species. Periodical DFT calculations on the $Fe_2(\mu$-O) site indicate that the ν_{as} (Fe–O–Fe) = 878 cm^{-1}, which agrees well with the *in situ* UV resonance Raman result. For the active $Fe_2(\mu$-$O)_2$ site and Fe-methoxide species, the calculated ν_s ($Fe_2(\mu$-$O)_2$) (746 cm^{-1}) and ν_s (C–O) (1067 cm^{-1}) and ^{18}O-isotopic shifts (−24 and −29 cm^{-1}, respectively) are also consistent with the experimentally observed values for these vibrations ν_s ($Fe_2(\mu$-$O)_2$) = 730 cm^{-1}, ($\Delta(^{18}O) = -25$ cm^{-1}) and ν_s (C–O) = 1095 cm^{-1}, ($\Delta(^{18}O) = -15$ cm^{-1}), respectively (Fig. 5). Consequently, the DFT calculations exactly reproduce the observed *in situ* resonance Raman results, which further confirm that the active iron site for N_2O decomposition is an $Fe_2(\mu$-O) site and the active iron site for methane oxidation is an $Fe_2(\mu$-$O)_2$ site.

4. Conclusions

In summary, we identified the structure of the active iron site for N_2O decomposition in Fe/ZSM-35 and the structural changes upon exposing the active iron site to N_2O. *In situ* UV resonance Raman and Mössbauer spectra results reveal that the active iron site responsible for direct N_2O decomposition is an $Fe_2(\mu$-O) site, giving a feature UV Raman band at 875 cm^{-1}. *In situ* visible resonance Raman spectra suggest that an $Fe_2(\mu$-$O)_2$ site exhibiting a characteristic Raman band at 730 cm^{-1} is formed upon exposure of the active $Fe_2(\mu$-O) site to N_2O. The $Fe_2(\mu$-$O)_2$ site can react with methane to produce methoxide species at room temperature, which mimics the biocatalysis of sMMO.

Acknowledgments

This work was supported financially by the Programme Strategic Scientific Alliances between China and the Netherlands (Grant

2008DFB50130), National Basic Research Program of China or 973 Program (Grant 2009CB623507) and National Natural Science Foundation of China (NSFC, No. 21173213).

Appendix A. Supplementary material

Supplementary data associated with this article can be found, in the online version, at http://dx.doi.org/10.1016/j.jcat.2013.01.023.

References

[1] I. Malpartida, E. Ivanova, M. Mihaylov, K. Hadjiivanov, V. Blasin-Aubé, O. Marie, M. Daturi, Catal. Today 149 (2010) 295.
[2] K. Jiša, J. Novakova, M. Schwarze, A. Vondrova, S. Sklenak, Z. Sobalik, J. Catal. 262 (2009) 27.
[3] S.S. Shevade, B.S. Rao, Catal. Lett. 66 (2000) 99.
[4] S. Sklenak, P.C. Andrikopoulos, B. Boekfa, B. Jansang, J. Nováková, L. Benco, T. Bucko, J. Hafner, J. Dděček, Z. Sobalík, J. Catal. 272 (2010) 262.
[5] V. Blasin-Aubé, O. Marie, J. Saussey, A. Plesniar, M. Daturi, N. Nguyen, C. Hamon, M. Mihaylov, E. Ivanova, K. Hadjiivanov, J. Phys. Chem. C 113 (2009) 8387.
[6] S. Bordiga, R. Buzzoni, F. Geobaldo, C. Lamberti, E. Giamello, A. Zecchina, G. Leofanti, G. Petrini, G. Tozzola, G. Vlaic, J. Catal. 158 (1996) 486.
[7] M. Schwidder, M.S. Kumar, K. Klementiev, M.M. Pohl, A. Brückner, W. Grünert, J. Catal. 231 (2005) 314.
[8] C. Li, G. Xiong, Q. Xin, J. Liu, P. Ying, Z. Feng, J. Li, W. Yang, Y. Wang, G. Wang, X. Liu, M. Lin, X. Wang, E. Min, Angew. Chem. Int. Ed. 38 (1999) 2220.
[9] J.S. Woertink, P.J. Smeets, M.H. Groothaert, M.A. Vance, B.F. Sels, R.A. Schoonheydt, E.I. Solomon, PNAS 106 (2009) 18908.
[10] L. Kiwi-Minsker, D.A. Bulushev, A. Renken, J. Catal. 219 (2003) 273.
[11] M.J. Frisch, G.W. Trucks, H.B. Schlegel, G.E. Scuseria, M.A. Robb, J.R. Cheeseman, J.A. Montgomery, Jr., T. Vreven, K.N. Kudin, J.C. Burant, J.M. Millam, S.S. Iyengar, J. Tomasi, V. Barone, B. Mennucci, M. Cossi, G. Scalmani, N. Rega, G.A. Petersson, H. Nakatsuji, M. Hada, M. Ehara, K. Toyota, R. Fukuda, J. Hasegawa, M. Ishida, T. Nakajima, Y. Honda, O. Kitao, H. Nakai, M. Klene, X. Li, J.E. Knox, H.P. Hratchian, J.B. Cross, C. Adamo, J. Jaramillo, R. Gomperts, R.E. Stratmann, O. Yazyev, A.J. Austin, R. Cammi, C. Pomelli, J.W. Ochterski, P.Y. Ayala, K. Morokuma, G.A. Voth, P. Salvador, J.J. Dannenberg, V.G. Zakrzewski, S. Dapprich, A.D. Daniels, M.C. Strain, O. Farkas, D.K. Malick, A.D. Rabuck, K. Raghavachari, J.B. Foresman, J.V. Ortiz, Q. Cui, A.G. Baboul, S. Clifford, J. Cioslowski, B.B. Stefanov, G. Liu, A. Liashenko, P. Piskorz, I. Komaromi, R.L. Martin, D.J. Fox, T. Keith, M.A. Al-Laham, C.Y. Peng, A. Nanayakkara, M. Challacombe, P.M.W. Gill, B. Johnson, W. Chen, M.W. Wong, C. Gonzalez, J.A. Pople, Gaussian 03; Gaussian, Inc., Pittsburgh, PA, 2003.
[12] A.D. Becke, Phys. Rev. A 38 (1988) 3098.
[13] C. Lee, W. Yang, R.G. Parr, Phys. Rev. B 37 (1988) 785.
[14] I.J. Pickering, P.J. Maddox, J.M. Thomas, A.K. Cheetham, J. Catal. 119 (1989) 261.
[15] P.K. Dutta, K.M. Rao, J.Y. Park, J. Phys. Chem. 95 (1991) 6654.
[16] P.K. Dutta, K.M. Rao, J.Y. Park, Langmuir 8 (1992) 722.
[17] Y. Suzuki, T. Wakihara, K. Itabashi, M. Ogura, T. Okubo, Top. Catal. 52 (2009) 67.
[18] K. Sun, F. Fan, H. Xia, Z. Feng, W.–X. Li, C. Li, J. Phys. Chem. C 112 (2008) 16036.
[19] C. Li, J. Catal. 216 (2003) 203.
[20] F. Fan, K. Sun, Z. Feng, H. Xia, B. Han, Y. Lian, P. Ying, C. Li, Chem. Eur. J. 15 (2009) 3268.
[21] L. Que Jr., W.B. Tolman, Angew. Chem. Int. Ed. 41 (2002) 1114.
[22] D.M. Kurtz Jr., Chem. Rev. 90 (1990) 585.
[23] M. Costas, M.P. Mehn, M.P. Jensen, L. Que Jr., Chem. Rev. 104 (2004) 939.
[24] A. Meagher, V. Nair, R. Szostak, Zeolites 8 (1988) 3.
[25] R. Kumar, S.K. Date, E. Bill, A. Trautwein, Zeolites 11 (1991) 211.
[26] K. Lázár, G. Lejeune, R.K. Ahedi, S.S. Shevade, A.N. Kotasthane, J. Phys. Chem. B 102 (1998) 4865.
[27] K. Lázár, A.N. Kotasthane, P. Fejes, Catal. Lett. 57 (1999) 171.
[28] K.A. Dubkov, N.S. Ovanesyan, 1.A.A. Shteinman, E.V. Starokon, G.I. Panov, J. Catal. 207 (2002) 341.
[29] R.L. Garten, W.N. Delgass, M. Boudart, J. Catal. 18 (1970) 90.
[30] L. Guczi, K. Lázár, React. Kinet. Catal. Lett. 96 (2009) 335.
[31] D.L.A. de Faria, S. Venâncio Silva, M.T. de Oliveira, J. Raman Spectrosc. 28 (1997) 873.
[32] J. Nováková, M. Lhotka, Z. Tvarůžková, Z. Sobalík, Catal. Lett. 83 (2002) 215.
[33] J. Nováková, M. Schwarze, Z. Sobalík, Catal. Lett. 104 (2005) 157.
[34] I.E. Wachs, Top. Catal. 8 (1999) 57.